Design and performance of liquid hydrogen fueled aircraft for year 2050 EIS

33RD CONGRESS
OF THE INTERNATIONAL COUNCIL
OF THE AERONAUTICAL SCIENCES
STOCKHOLM, SWEDEN, 4-9 SEPTEMBER, 2022

ICAS 2022 SWEDEN

DESIGN AND PERFORMANCE OF LIQUID HYDROGEN FUELLED AIRCRAFT FOR YEAR 2050 EIS

Carlos Xisto[1] & Anders Lundbladh[2]

[1]1Chalmers University of Technology, Department of Mechanics and Maritime Sciences, Gothenburg, SE-41296, Sweden
[2]GKN Aerospace, Trollhättan, SE-46138, Sweden

Abstract

The present paper reports on the investigation of long-range LH_2 aircraft concepts for year 2050 entry into service. The paper attempts to identify the limitations set by the LH_2 storage technology when targeting typical design payload-range missions. In particular, the paper aims at providing a reasonable estimate of the upper efficiency levels set by low-weight rigid cell foam insulated tank technology, when integrated in a conventionally shaped airframe. Additionally, a sensitivity study on the gravimetric efficiency of the tanks will be carried out, to identify the required roadmap for LH_2 storage technology that is compliant with the typical long range mission requirements. Results for the different LH_2 aircraft are compared with a year 2020 and year 2050 reference aircraft fueled with conventional jet-A.

Keywords: Aircraft; LH_2; Cryo-tank; 2050EIS

1. Introduction

In order to meet the ambitious environmental targets set by the Paris Agreement, new sustainable carbon neutral aviation fuels need to be introduced. The high gravimetric energy density of hydrogen, makes it a prime candidate for a future aviation fuel. However, the associated poor volumetric energy density requires an increased aircraft volume and associated penalty in aerodynamic performance. The required volume occupied by the hydrogen fuel can be decreased in half, if stored in its liquid form. This however requires that the liquid hydrogen (LH_2) is kept at cryogenic temperatures, requiring heavy insulation technology that increases the aircraft operating empty weight. In an attempt to mitigate some the aforementioned drawbacks, we very often see concepts that rely on more disruptive aerodynamic shapes such as blended wing body aircraft to more efficiently integrated the bulkier fuel tanks in the fuselage. These concepts are indeed interesting and seem to offer several advantages over conventional tube and wing configurations [12]. They do however increase the risk associated with the introduction of new technology in a sector, where the requirements for reliability, safety and operability are extremely stringent.

In the present paper we investigate aircraft concepts for year 2050 relying on a “low-risk” tube and wing arrangement, where the LH_2 tanks are externally mounted above the fuselage. For the present paper, only long range aircraft concepts are investigated in an attempt to identify the limitations set by the heavy LH_2 storage technology when targeting typical design payload-range missions. First, a reference aircraft for year 2020 is developed based on a stretched version of an existing Pacelab APD Airbus A350-1000 model. After, a baseline aircraft for year 2050 is proposed, assuming improved technology with respect to weight, aerodynamics and engine performance. The year 2050 aircraft is later re-designed for LH_2. The paper aims at providing a reasonable estimate of the upper efficiency levels set by low-weight rigid cell foam insulated tank technology, when integrated in a conventionally shaped airframe. Additionally, a sensitivity study on the gravimetric efficiency will be carried out, to identify the required roadmap for LH_2 storage technology that is compliant with the typical long range mission requirements.

Table 1 – Aircraft top level requirements.

General requirements	
Entry into service	2050
Design Range	7500 NM
PAX (two-class)	414
Typical passenger weight	115 kg
Passenger weight for max load	166 kg
Airport compatibility	Code E
Take-off and Landing	
TOFL (MTOW, sea level, ISA)	3048 m
Time to climn (from 1500 ft, ISA)	25 min
Approach speed (MLW, sea level, ISA)	$<$ 140 KCAS
LFL (MLW, ISA)	1768 m
Cruise	
Initial cruise altitude (ISA+10)	at least FL330
Design cruise Mach number	at least M0.82
Max cruise altitude	FL410

2. Aircraft top level requirements and year 2020 reference

The aircraft top level requirements are listed in table 1, these were derived by experts in the early stage of the H2020 EnableH2 project [12].

The year 2020 reference (2020) aircraft is based on a hypothetical stretched version of an airbus A350-1000 aircraft. The rationale behind the choice of developing a new aircraft for Y2020 is that the -1000 cannot comply with the required range-capacity, specified in Table 1, of 414 PAX in a two-class cabin configuration comprising a 6 abreast business class with pitch equal to 1.52 m and a 9 abreast economy class with pitch equal 0.81 cm. Therefore, for the existing -1000 configuration, 39 additional economy and 6 additional business seats are included. An existing aircraft model representing the A350-1000 is therefore modified to include the additional capacity, the following assumptions are made when developing the 2020 model:

- The fuselage is increased by 5.6 m;
- The span is kept constant;
- The aircraft and engine thrust-to-weight ratio are kept constant;
- The ratios MRW/MTOW and MZFW/MLW and the control surfaces volume coefficients are keep constant, see Table 2;
- The wing loading is set to 735 kg/m^2 and the value was derived from extrapolation from the 350-900 and 350-1000 data;
- The chord is slightly increased to meet the new wing loading and MTOW.
- The wing position relative to the nose is increase using the following linear relation:

$$\Delta L_{wing,1000-2020} = \frac{\Delta L_{wing,900-1000}}{\Delta L_{stretch,900-1000}} \cdot \Delta L_{stretch,1000-2020} \tag{1}$$

  where ΔL_{wing} is the variation in distance between the wing and the nose and $\Delta L_{stretch}$ is the variation in fuselage length.

It is noted that the year 2020 reference should represent the state-of-the-art flying technology. Hence, the aircraft top level performance, such as wing loading or thrust-to-weight ratio will not be optimized with respect to fuel burn. Still, the extrapolation of wing data from the -900 and -1000 designs requires additional clarifications. Existing aircraft public data was analysed leading to the conclusion that a

Table 2 – Sizing parameters used for the year 2020 reference aircraft.

Parameter	2020
Wing loading [kg/m^2]	735
Aircraft thrust-to-weight ratio [-]	0.279
Wing span [m]	64.74
Fin volume coefficient [-]	0.051
Stabilizer volume coefficient [-]	0.70
Engine thrust-to-weight ratio ($SLS/mass_{dry}$) [-]	5.6
MRW/MTOW [%]	100.3
MZFW/MLW [%]	94.5

value of 735 kg/m^2 is feasible in present day aircraft. Moreover, the low speed performance of the wing is verified to comply with the design requirements. The sizing parameters used for the year 2020 reference aircraft are summarized in Table 2. The fin volume coefficient is calculated by dividing the product of the respective control surface wetted area and moment arm (distance from the control surface quarter chord to the wing quarter chord) with the product between wing area and wing span. In the definition of the stabilizer volume coefficient the mean aerodynamic chord should be used instead of the wing span.

3. Assumptions on technology improvements for year 2050

Two long-range aircraft configurations projected from the year 2020 model are proposed for year 2050 entry into service. The first aircraft is assumed to be fuelled with conventional jet-A or replacement drop-in (baseline), and the second aircraft with liquid hydrogen (LH_2). The technology improvement projections are applied in the form of coefficients that modify the weight and the aerodynamic performance of each aircraft. The technology improvement coefficients are based in findings from the ULTIMATE project [9] and from public reports such as the one provided by IATA [10].

- A reduction of 5% in structural mass is assumed due to an increased usage of carbon fibre reinforced polymer (wing, fin, stabilizer, fuselage, landing gear, nacelles). The 5% comes from the fact that the A350 is already made of approximately 50% of composite material resulting in a structural weight reduction of 15% when compared to previous generation aircraft (A330: 12% composite).
- Interior furnishing: in the ULTIMATE project a 15% reduction was assumed for the furnishing weight [9]. However, such assumption was relative to year 2000 reference technology. For the present analysis we assume that from 2020 up to 2050 a 7.5% reduction in interior furnishing is achievable.
- Regarding the Gust Manoeuvre Load Alleviation/Manoeuvre load alleviation (GLA/MLA). As specified in the ULTIMATE project a 5% reduction in wing structural mass is expected by alleviating the bending moment at the wing root. It is noted that such technology is already available in the existing A350 aircraft. Still, second/third generation technology is expected to lead to a similar reduction of wing mass.
- Regarding the integration of riblets, here the ULTIMATE project assumption is employed, implying that an 8% reduction is possible in 70% of the fuselage skin friction.
- Shock control bump technology is assumed for wave drag reduction. Looking into reference [13] there is a 3% overall drag reduction potential from shock control bump technology or novel configurations. Such improvement translates into 14% in wave drag reduction when applied into the A350 derived model.
- High aspect ratio wings will be considered, and dedicated trade-studies will be performed to determine what is the optimum aspect ratio for each configuration. The aircraft for year 2050

Table 3 – Final set of improvement coefficients used for the different year 2050 aircraft models

Technology	Impact	Parameter impacted
Carbon fiber reinforced polymer	-5%	Structural mass
Light furnishing	-7.5%	Furnishing mass
MLA/GLA (load alleviation)	-3%	Wing mass
Riblets	-5.6%	Skin friction fuselage
Shock control bump	-14%	CD_{wave}
Improved engine materials	+28%	Engine thrust-to-weight ratio

is also assumed to include foldable wing technology to allow for high aspect ratio wings and comply with the Code E airport compatibility. The weight of the fold mechanism is calculated using the methodology proposed by [8].

$$\frac{F_s}{\mathrm{TOGW}} = \frac{1}{2} \cdot \left(1 - \frac{2}{\pi} \cdot \eta_{\mathrm{fold}} \cdot \sqrt{1 - \eta_{\mathrm{fold}}^2} - \frac{2}{\pi} \sin^{-1}\left(\eta_{\mathrm{fold}}\right)\right) \tag{2}$$

where F_s is the shear force acting on the folding line, and η_{fold} is the folding line to half-span ratio. The weight of the folding mechanism can be finally estimated:

$$\frac{W_{\mathrm{fold}}}{\mathrm{TOGW}} = 0.07 \cdot \frac{F_s}{\mathrm{TOGW}} \tag{3}$$

- Increased laminar flow area in the nacelles is already considered for the baseline A350 [6]. Still, for the present analysis it is considered that there is a high degree of uncertainty on estimating the benefit of increased laminar flow region in the aircraft, by applying active or passive flow control mechanisms. Therefore, for the year 2050 long range baseline aircraft no improvement arising from laminar flow is considered.

The final improvements used to setup the year 2050 models are summarized in Table 3. Improvements at an engine level are also introduced as factors on fuel burn, see section 5.for more details. Moreover, the engine thrust-to-weight ratio was increased to 7.16 following the projections of the ULTIMATE project [11].

4. LH_2 Tank sizing and installation

The thermodynamic and mechanical design procedure is based on the methods proposed by [2] for aluminium tanks with an insulation provided by rigid cell PVC. The procedure for a two-tank layout design is implemented in a python script as follows.

- First, in order to reduce frontal area, the maximum possible length for the front and aft tanks is selected, considering the estimated required engine debris gap presented in the previous section.
- Second, the fuel fraction per tank is calculated as function of the ratio between the length of the two tanks.
- After, the routine iterates on the required external diameter that accommodates the required fuel per tank at a given tank length.
- a thermodynamic calculation is carried out to estimate the require insulation thickness that satisfies the required boil-off rate. For the prescribed design mission it is expected that a boil-off corresponding to 2% of the tank capacity is acceptable.
- An external iteration loop is added to converge on the final fuel requirement and tank sizing, considering the boil-off rate and mission time.
- the code returns the tank + fuel + insulation weight.

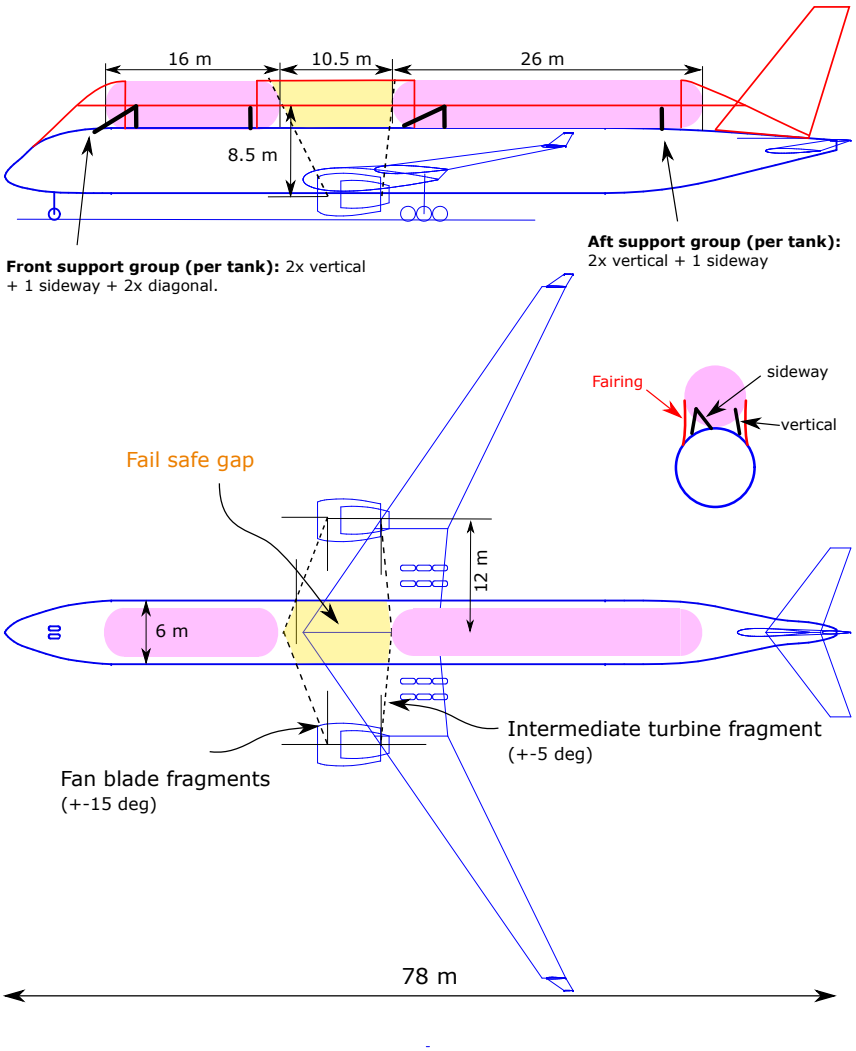

Figure 1 – Long-range aircraft with tanks mounted above the pressurized fuselage

- The support structure and fairing weight as well as total exposed area are finally calculated for the converged tank design.

The algorithm is run for various fuel requirements and debris gap lengths in order to generate correlations for system weight and added drag that can be easily implemented into APD Pacelab for aircraft performance calculations.

4.1 Tank installation

The modelling strategy of the year 2050 LH_2 aircraft requires further details, more specifically concerning LH_2 tank layout, fairing and support structures. The selected tank configurations is illustrated in Figure 1. The image shows a tank configuration including two tanks mounted on top of the fuselage. In order to reduce interference drag, fairing (red line) is included on the front, back and sides of the tanks. Additional fairing is included to cover the gap defined by the front and aft tanks.
The exposed wetted area is computed by defining front and aft half ellipsoids with width and height equal to tank diameter. The lateral fairing connecting the side of the tank to the side of aircraft is defined as an unfold half cylinder with diameter equal to tank diameter. The fairing covering the gap defined by the front and aft tanks is defined as a cylinder with diameter equal to tank diameter and length equal to gap length plus the tank diameter. For the purpose of weight saving the upper half of the tanks is not covered by any fairing. The area of the fuselage covered by the fairing is subtracted and not considered in the aerodynamic performance of the aircraft.
In the present work the weight of the fairing is simply estimated to be 15 kg/m^2 of wetted area. The

uncertainty for fairing weight is high, since it requires an adequate investigation of different structural aspects. Still, the proposed number is approximately half of typical civil aircraft fuselage and deemed adequate for the present analysis.
The support structure for each tank is also depicted in Figure 1. It is composed of front and aft support groups each containing a pair of vertical support beams and one sideway beam to resist sideways movement of the tank. Two struts going diagonally forward on each side of the tank are also added to resist forward loads during landing. For sizing purposes, the FAR 25.561 regulation [3] is used and therefore the structure is required to withstand the ultimate loads of 9g forward (diagonal support) and 6g downward (vertical support) in the case of emergency landing. For such conditions the tanks are assumed to be filled with fuel. The beams are made of 7075 Aluminium with an assumed yield strength of 300 MPa and density equal to 2810 kg/m3.
A gap between the front and aft tanks is assumed to include an engine debris fail safe area. As specified in the FAA-AC-20-128A [1], the fragment spread angle measured, fore and aft, from the centre of rotation at engine centreline is +-15 degrees for fan blade fragments and +-5 degrees for turbine fragments. A diagram, containing the estimated gap for a given aircraft design and acceptable tank lengths is provided in Fig. 1. It is noted that every design will produce different gap lengths, for example increasing the span will move the engines away from the fuselage which will increase the required gap size. Therefore, this parameter is included in the design loop assuming a total usable length of 56 m.
The layout in Fig.1 results in an increased fuselage wetted area and consequent drag increase. However, the fitness ratio,

$$\lambda = \frac{L}{\sqrt{4A_c/\pi}}, \tag{4}$$

also increases due to an increase in fuselage cross-sectional area, A_c, for a constant fuselage length, L. Hence, the drag penalty incurring from mounting the tanks above the fuselage is not only restricted to an increase wetted area. To compensate for this effect, the form-factor is corrected to include variations in fitness ratio:

$$C_{d,fuselage} = c_f \cdot S_{wet,fuselage} \cdot (1 + \phi_f), \tag{5}$$

where the variations in shape factor with fitness ratio can be estimated as [14]:

$$\phi_f = \frac{2.2}{\lambda^{1.5}} + \frac{3.8}{\lambda^3}. \tag{6}$$

5. Propulsion system

The propulsion system is based on a recuperative cycle modeled in Chalmers in-house aeroengine performance tool GESTPAN (GEneral Stationary and Transient Propulsion ANalsysis) [7]. GESTPAN was recently extended for simulation with cryogenic fuels, including new post-combustion gas tables and the integration of real gas modeling using REFPROP to simulate the heat-exchange between the core and fuel flows [4].
The recuperative cycle architecture is illustrated in Fig. 2, where a two-pass cross-over tubular heat exchanger is placed at the exhaust to pre-heat the H_2 before combustion. Pre-heating the fuel allows to increase the fuel entalphy before combustion, effectively increasing the combustion heating value. As an example, assuming that the tank is filled with hydrogen at 25 K and the fuel absorbs heat up to a temperature of 800 K, entering the combustor. The heat added per kilogram of fuel (MJ/kg) corresponds to about 9% of the hydrogen lower fuel heating value (120 MJ/kg). Hence, theoretically in a loss free system, the maximum potential is a 9% reduction in specific fuel consumption (SFC). Hence, for the very high combustion efficiencies expected, there is an obvious gain from exchanging heat from the exhaust gases to the fuel. The cycle performance for three off-design point calculations (MTO - maximum take-off, MCL - maximum climb and MCR - maximum cruise) is listed in Table 4. The fuel temperature is affected by the heat-exchanger effectiveness, but also the pressure loss. In the end, the optimal effectiveness will need to account for installation effects such as heat-exchanger weight and penalty in drag due to increased engine frontal area. The performance listed in Table 4 is in accordance with the year 2050 gear-turbofan reference engine, modeled as part of the H2020 ULTIMATE project [11].

Table 4 – Propulsion system performance for year 2050 LH_2 engine with exhaust pre-heating.

	MTO	MCL	MCR
Altitude [ft]	0	35,000	37,000
Specific Thurst [m/s]	227	96	83
Mach number	0	0.84	0.85
ΔISA [K]	0	0.0	0.0
T_3 [K]	946	900	861
P_3 [bar]	59.0	29.0	23.4
T_4 [K]	1845	1777	1687
BPR	22	21.7	23.1
FPR	1.36	1.45	1.39
OPR	58.5	76.5	67.4
Pre-heater eff.	0.8	0.79	0.82
T_fuel [K]	646	570	552
SFC [mg/N-s]	1.87	4.35	4.34

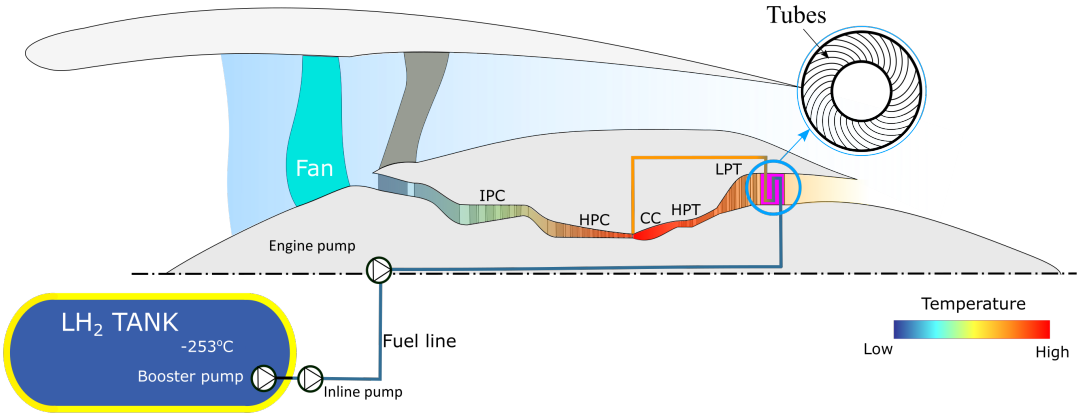

Figure 2 – Illustration of a cross-sectional meridional cut of a turbofan engine, including an exhaust fuel pre-heater. The fuel is stored at its boiling point in the cryogenic tank. IPC: Intermediate-pressure compressor; HPC: High-pressure compressor; HPT: High-pressure turbine; LPT: Low-pressure turbine.

Table 5 – Mission flight profile.

Initial climb up to 10,000 ft	250 CAS
Climb after 10,000 ft	300 CAS or Mach 0.84
Cruise	Mach 0.85
Descent	300 CAS or Mach 0.84
Contingency	5% trip fuel
Diversion	150 NM @ 25,000 ft
Hold	30 min @ 1,500 ft

6. Results

In the present section the results obtained for the different modelled aircraft are presented and discussed. The results are all obtained for the design mission of 414 PAX, 7500 NM following the flight profile characteristics specified in Table 5. The section starts with the sizing of year 2050 baseline aircraft (Jet-A) and the trade-study leading to the fuel-optimal configuration. After, the year 2050 LH_2 variant is optimized for fuel-burn and compared with the 2050 baseline. Finally, a tank technology sensitivity study is carried out to determine the impact of tank weight on the relative performance and sizing of the aircraft.

6.1 Year 2050 baseline aircraft

The work reported in this section is mainly concerned about defining the design mission fuel-optimal combination of wing-loading (WL) and thrust-to-weight (TW) ratio, that is compliant with the aircraft top-level requirements. We start by finding the optimum wing size by running a trade study of wing loading vs span. Lower values for wing loading increase the wing size resulting in increased empty weight and drag, but also lead to improved low speed performance, e.g. approach speed, stall speed. Another aspect that requires consideration in tube and wing aircraft, is that the fuel is stored inside the wing and therefore a higher wing loading, and resulting smaller wing leads to less fuel storage capacity. For a fixed wing loading, increasing the span leads to improved high-speed aerodynamics due to a decrease in induced drag. However, for fixed area wings, increasing the span leads to wing weight increase that in the present work will be further penalized due to the required wing folding-locking mechanism for spans above 65 m. The wing loading vs span trade study results are shown in Fig. 3-a) for the year 2050 Jet-A aircraft. The results show the computed relative fuel burn, including a grey shaded region that represents the fuel storage capacity constraint. The optimum design parameters are also plotted in red circles to illustrate what is the selected design for the wing configuration. A wing loading of about 724 kg/m^2 and a span of about 69 m gives the best fuel burn performance for the design mission of 7500 NM. In Fig. 3-b) the results of a relative mission fuel-burn are shown to determine the minimum fuel burn combination of wing-loading and thrust-to-weight. The results show that the minimum fuel burn is given for a thrust-to-weight ratio of 0.285.

6.2 2050 LH_2 aircraft

Again, now for the LH_2 aircraft, an optimum wing size is investigated by conducting a trade study of wing loading vs span. It is now noted that wing fuel capacity is no longer a constraint since the hydrogen is stored in tanks above the fuselage. On the other hand, constraints like approach speed and landing field length start to restrict the design. This is a particularity of the “landing heavy” LH_2 aircraft where the OEW/MTOW fraction of 0.688 is significantly higher than the one provided by the Jet-A 2050 counterpart (0.48). Figure 4-a) shows the results obtained for the wing-loading vs span trade study including the limiting factor set by the landing field length constraint. For this particular study the minimum fuel burn wing loading was limited to 608 kg/m^2. A similar WL vs T/W study to the one conducted for the Jet-A 2050 aircraft is performed for the LH_2 configuration, see Figure 4-b). For this particular study, the constraint set by the landing field length limits the maximum wing loading to approximately 608 kg/m^2, whereas the constraint set by the minimum cruise altitude limits the TW to approximately 0.31. The optimum design parameter combination leading to minimum fuel burn is plotted with a red dot.

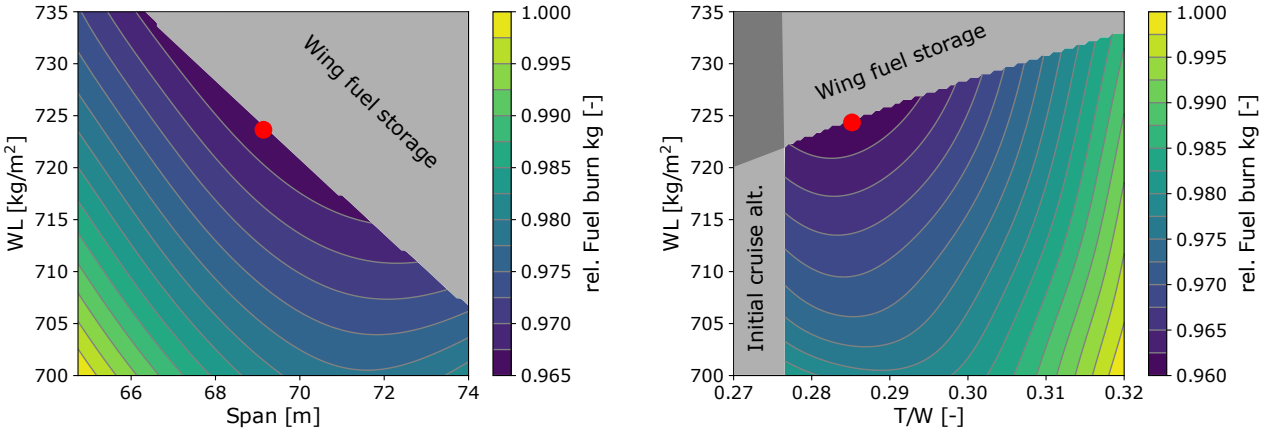

Figure 3 – Relative fuel burn results computed for the design mission of 7500 NM in the 2050 Jet-A aircraft. Fuel burn is referenced to the maximum value obtained for each trade study. Variation of mission relative fuel burn with: a) Wing loading vs. Span: b) Wing loading vs. Thrust-to-weight. The shaded areas are constraints set by the minimum initial cruise altitude of 33000 ft and minimum fuel storage capacity.

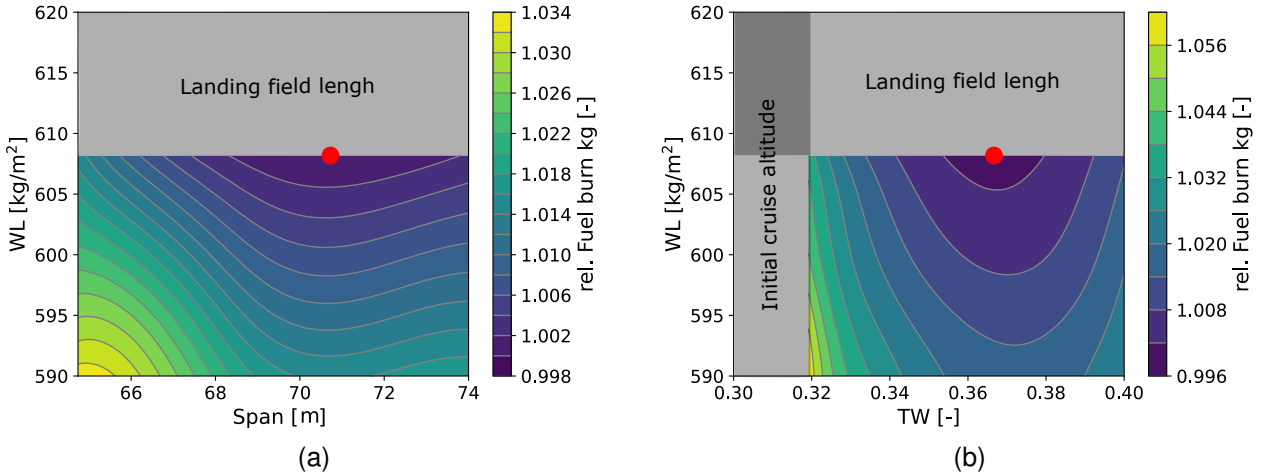

Figure 4 – a) Minimum fuel burn aircraft design in a wing loading vs Span plot for a thrust-to-weight ratio of 0.367. b) Minimum fuel burn aircraft design in a wing loading vs thrust-to-weight plot. The shaded areas are constraints set by the minimum initial cruise altitude of 33000 ft and maximum landing field length @MLW ISA of 1768 m.

Table 6 – Tank design parameters and performance for the LH_2 aircraft.

	Forward tank	Aft Tank
External diameter [m]	4.92	4.8
Length [m]	16	26
Tank mass [kg]	4,175	6,378
Insulation mass [kg]	1,939	2,579
Fuel mass [kg]	16,370	26,089
Volume (inc. insulation) [m^3]	273	434
Support structure mass [kg]	276	431
Mission boil-off [kg]	356	504
Engine fail safe gap [m]	10.5	
Fairing mass [kg]	10,500	
Exposed wetted area [m^2]	658	

Table 7 – Comparison between performance and design parameters for the year 2020 and 2050 aircraft.

	Jet-A 2020	Jet-A 2050	LH_2	LH_2/Jet-A (2050)
Mid-cruise L/D [-]	19.1	20.6	17.9	0.87
MTOW [kg]	345,600	293,700	285,600	0.97
MLW [kg]	251,190	234,000	280,600	1.20
OEW [kg]	167,700	142,300	196,450	1,29
Block fuel [kg]	118,900	93,900	37,500	0.44
Fuel weight inc. reserves [kg]	130,500	93,900	41,600	0.44
Wing area [m^2]	475	410	475	1.16
T/W [-]	0.279	0.285	0.367	1.16
Wing loading [kg/m^2]	735	724	608	0.84
Span [m]	64.74	69	70.5	1.02
Energy use [MJ/PAX km]	0.893	0.641	0.782	1.22

The respective tank design parameters and performance for the fuel optimal aircraft are listed in Table 6. The results show that for the assumed tank storage technology the PVC insulation results in an extremely light solution. The combined mass of the tank and insulation is only about 35% of the fuel mass. The gravimetric density of the storage system is therefore about 73 MJ/kg. This is very much in contrast with today's under-development technology for commuter aircraft where the gravimetric index is belived to be about 0.2 [5] (see eq. 7), resulting in an effective gravimetric density of 24 MJ/kg and a ratio between fuel mass to tank mass of about four. As a reminder, the gravimetric density of Jet-A fuel is about 43 MJ/kg, considering that the fuel do not add any extra weight to the wing structure.

A final comparison between the year 2020 reference and year 2050 Jet-A and LH_2 variants is provided in Table 7. The ratio between the LH_2 and 2050 Jet-A aircraft performance parameters is given in the last column. Results show that the most energy efficient option is the Jet-A (or drop-in replacement) year 2050 aircraft. The energy consumption for the LH_2 variant increases by 22%, still providing a more efficient solution when compared to the year 2020 reference, this is however heavily dependent on the availability of light weight rigid cell foam insulation technology. The operational empty weight (OEW) increases by about 29% resulting in an heavier aircraft during landing, requiring larger wings to meet the low speed performance requirements. The aerodynamic performance is clearly penalized by the larger LH_2 tanks, increasing the wetted area and decreasing the fuselage fitness ratio. The thrust-to-weight ratio is required to increase in order to overcome the added drag and to allow for the required minimum cruise altitude.

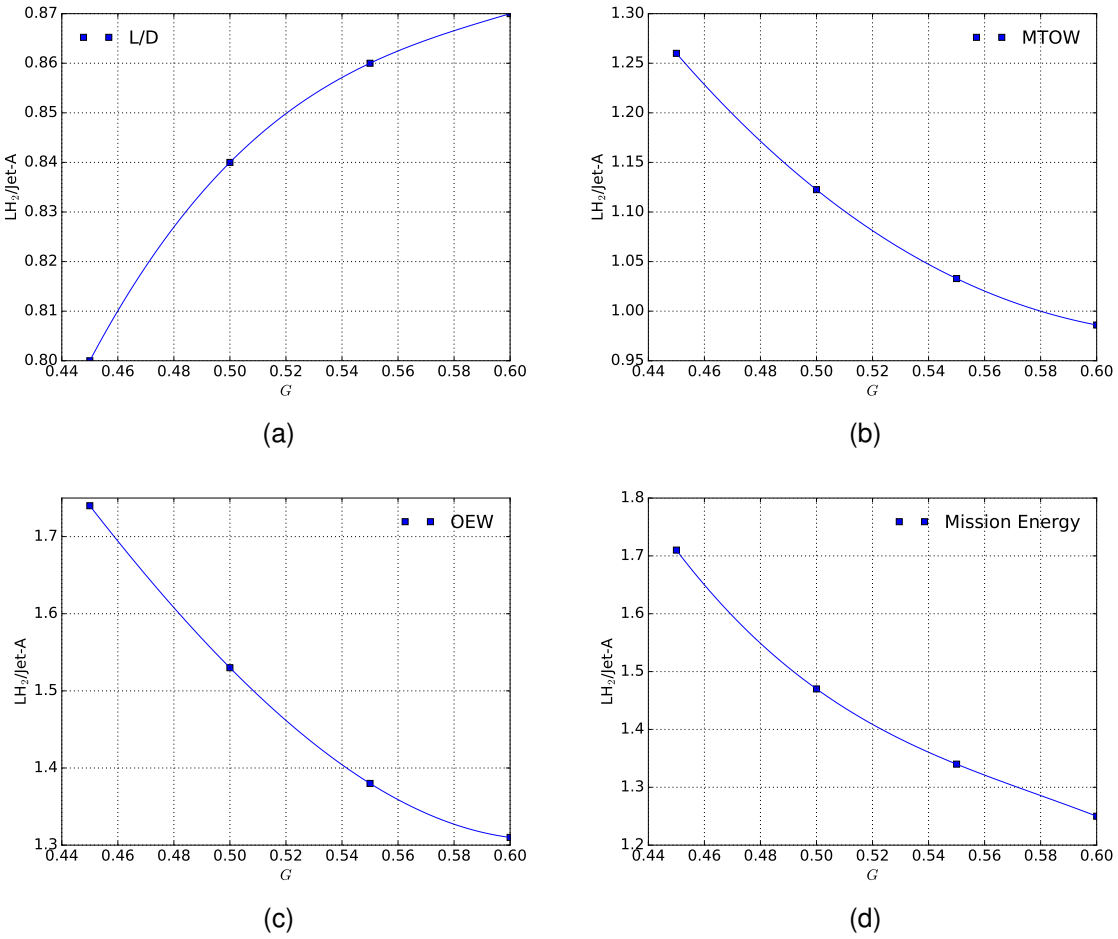

Figure 5 – Results obtained for the variation of relative performance parameters between the LH_2 and Jet-A 2050 counterpart.

6.3 Sensitivity study on gravimetric index

The assumption of light weight rigid cell foam insulation technology carries a great deal of uncertainty. Hence, a sensitivity study is carried out to evaluate the impact of increasing tank weight on the aircraft performance metrics. The parameter used to represent insulation technology is the gravimetric index:

$$G = \frac{m_{fuel}}{(m_{tank+fairing+structure} + m_{fuel})}, \tag{7}$$

which simply gives the fraction of usable specific energy. The data in Table 6 results in a gravimetric index of about $G = 0.7$, excluding fairing weight, and about $G = 0.6$ including fairing weight. This is much higher than today's under-development technology of $G = 0.2$. In the present study we vary the gravimetric index between 0.45 and 0.6 to illustrate the rapid deterioration in performance and also to set the limit for the acceptable range for the relative mass of the tank.

Figure 5 show the results obtained for the variation of relative performance parameters between the LH_2 and Jet-A 2050 counterpart. Reductions in the gravimetric index lead to rapid increases in OEW and sharp decreases in aerodynamic performance, leading to energy consumption increases of up to 70% for $G = 0.45$. For the present design mission, the large payload (414 PAX) and substantial range 7500 NM require a large fuel weight ratio, which associated with heavy tanks lead to large performance deterioration. The results here show that a gravimetric index of 0.5 is required for a mission energy consumption increase of 50%.

7. Conclusion

The present paper addressed the challenges of designing hydrogen fueled long range aircraft. The aircraft concept proposed in this paper is not very challenging by itself, since it relies on fuel tanks

being externally mounted above the pressurized fuselage. The tanks could be partially covered to reduce interference drag and the supporting system can probably be built in a very simple way. Also, this arrangement can be used to shift the aircraft center-of-gravity by moving the fuel around between the tanks. However, mounting the tanks above the fuselage should require careful planning and construction to avoid fuel spillage in the passenger cabin in the event of crash landing.
Regarding performance, the impact that the increased weight and volume of the tanks have in key aircraft performance parameters is substantial, leading to an increase in energy consumption between 20% to 70% depending on the storage technology employed. The main conclusion is that long-range LH_2 aircraft, although theoretically possible, suffer from major drawbacks due to large fuel weight ratios and require ultra-light tank technology. In particular, for similar ranges of today's best in class long-range aircraft, technology with a gravimetric index of about 0.5 (ratio between tank and fuel masses is equal to one) is required to fulfil the design mission at a cost of 50% increase in energy consumption. Hence, even unproven (today's best ratio between tank and fuel masses is believed to be 4) light weight technology carries a heavy penalty in terms of energy demand, showing that long-range application of hydrogen in aviation is not possible in the near or medium term future.

8. Acknowledgements

The E.U. financially supports this work under the "ENABLEH2 – Enabling cryogenic hydrogen-based CO2 free air transport" Project co-funded by the European Commission within the Horizon 2020 Programme (2014-2020) under Grant Agreement no. 769241.

9. Contact Author Email Address

mailto: carlos.xisto@chalmers.se

10. Copyright Statement

References

[1] AC 20-128A - design considerations for minimizing hazards caused by uncontained turbine engine and auxiliary power unit rotor failure document information. Technical report, ANM-114, Northwest Mountain Region - Transport Airplane Directorate, 1997.

[2] *Cryogenic Fuel Storage Modelling and Optimisation for Aircraft Applications*, volume Volume 6: Ceramics and Ceramic Composites; Coal, Biomass, Hydrogen, and Alternative Fuels; Microturbines, Turbochargers, and Small Turbomachines of *Turbo Expo: Power for Land, Sea, and Air*, 06 2021. V006T03A001.

[3] FAR25.561 - airworthiness standards: Transport category airplanes; subpart c - structure emergency landing conditions; 25.561 general. Technical report, Federal Aviation Administration, 2022.

[4] Hamidreza Abedi, Carlos Xisto, Isak Jonsson, Tomas Grönstedt, and Andrew Rolt. Preliminary analysis of compression system integrated heat management concepts using lh2-based parametric gas turbine model. *Aerospace*, 9(4), 2022.

[5] Fuel Cells and Hydrogen 2 Joint Undertaking. *Hydrogen-powered aviation : a fact-based study of hydrogen technology, economics, and climate impact by 2050*. Publications Office, 2020.

[6] O. Criou. A350 xwb family and technologies. In *Airbus presentation at Hamburg university of applied sciences*, 2007.

[7] Tomas Grönstedt. *Development of methods for analysis and optimization of complex jet engine systems*. Ph.d. thesis, Chalmers University of Technology, Gothenburg, Sweden, 2000.

[8] Ohad Gur, Manav Bhatia, Joseph A. Schetz, William H. Mason, Rakesh K. Kapania, and Dimitri N. Mavris. Design optimization of a truss-braced-wing transonic transport aircraft. *Journal of Aircraft*, 47(6):1907–1917, 2010.

[9] Philipp Heinemann, Periklis Panagiotou, Patrick Vratny, Sascha Kaiser, Mirko Hornung, and Kyros Yakinthos. Advanced tube and wing aircraft for year 2050 timeframe. In *55th AIAA Aerospace Sciences Meeting, Grapevine, Texas.*, number AIAA 2017-1390, 2017.

[10] IATA. *Aircraft Technology Roadmap to 2050*. 2019.

[11] Francesco S. Mastropierro, Joshua Sebastiampillai, Florian Jacob, and Andrew Rolt. Modeling Geared Turbofan and Open Rotor Engine Performance for Year-2050 Long-Range and Short-Range Aircraft. *Journal of Engineering for Gas Turbines and Power*, 142(4), 02 2020. 041016.

[12] Pavlos Rompokos, Andrew Rolt, Devaiah Nalianda, Askin T. Isikveren, Capucine Senné, Tomas Gronstedt, and Hamidreza Abedi. Synergistic technology combinations for future commercial aircraft using liquid hydrogen. *J. Eng. Gas Turbines Power*, 2021.

[13] G. Schrauf. Katnet key aerodynamic technologies for aircraft performance improvement. In *Fifth Community Aeronautical Days, Vienna, Austria*, 2006.

[14] Egbert Torenbeek. *Synthesis of Subsonic Airplane Design*. Delft University Press, Delft, 1982.